Publications of the Astronomical Society of Australia (2018), **35**, e037, 13 pages
doi:10.1017/pasa.2018.45

CAMBRIDGE UNIVERSITY PRESS

Research Paper

A correlation between *GALEX* FUV magnitude and chromospheric activity among red giant stars

Graeme H. Smith
UCO/Lick Observatory, University of California, Santa Cruz, CA 95064, USA

Abstract

It is shown that upon combining *GALEX* far-ultraviolet and Johnson *B* magnitudes a resultant FUV–*B* colour can be obtained that for red giant stars of luminosity classes III and II correlates well with chromospheric emission in the cores of the Mg II *h* and *k* lines. Giant stars throughout the colour range $0.8 \leq B–V \leq 1.6$ exhibit such a phenomenon. The main result of this paper is to show that *GALEX* far-ultraviolet photometry can provide information about the degree of chromospheric activity among red giant stars, and as such may offer a tool for surveying the evolution of chromospheric activity from the main sequence into the red giant phases of stellar evolution.

Keywords: stars: activity – stars: chromospheres – stars: late-type

(Received 02 May 2018; revised 28 August 2018; accepted 10 October 2018)

1. Introduction

Among dwarf stars in the spectral type range from mid-F to K, there is a correspondence between far-ultraviolet (FUV) brightness and the level of both chromospheric and coronal activity (e.g., Smith & Redenbaugh 2010; Findeisen, Hillenbrand, & Soderblom 2011; Murgas et al. 2013; Shkolnik et al. 2014; Smith, Hargrave, & Eckholm 2017), as traced by indicators such as Ca II H and K emission, Mg II *h* and *k* emission, and soft X-ray luminosity. A similar correspondence among M dwarfs has been detailed by Shkolnik et al. (2014) and Shkolnik & Barman (2014). The aim of this paper is to extend the evidence for a chromospheric-activity–FUV relation to red giant stars. The basis for this study is FUV photometry obtained from the *GALEX* satellite (Morrissey et al. 2005, 2007), combined with a data set of homogeneous measurements of the strength of the chromospheric emission in the cores of the Mg II *h* and *k* lines from Pérez Martínez, Schröder, & Cuntz (2011; PM11).

2. Data compilation

The work of Pérez Martínez et al. (2011) has provided a valuable compendium of chromospheric λ2800 Mg II emission line strengths for a sample of evolved giant stars, all measured from high-resolution *IUE* spectra in a homogeneous manner. The parameter derived by PM11 is the combined flux at the stellar surface in the Mg II *h* + *k* emission lines, which will be denoted herein as $F_{\rm mgii}$. PM11 give their measured surface fluxes in units of mW m^{-2}. Two values of the stellar surface flux were derived by PM11 by combining the flux measured at Earth from the *IUE* spectra with two different values of stellar effective temperature based on the *B*–*V* and *V*–*K* colours, and bolometric corrections applied to *V* and *K* magnitudes. In this paper a straight average of the two $F_{\rm mgii}$ values from PM11 has been adopted for each star. Additionally, a ratio of the Mg II *h* + *k* surface flux to the bolometric surface flux has been calculated for each star, using the formula

$$\log\,(F_{\rm mgii}/F_{\rm bol}) = \log F_{\rm mgii} - \log\,(\sigma T_{\rm eff}^4). \quad (1)$$

The value of the effective temperature used here is the mean of the values from PM11 that are based separately on *B*–*V* and *V*–*K* colours.

Trigonometric parallaxes were obtained from the SIMBAD Astronomical Database (Wenger et al. 2000) for all giants in the PM11 sample, these in turn typically coming from the *Gaia* Data Release 2 (*Gaia* Collaboration et al. 2018; Lindegren et al. 2018). In some cases the parallaxes are from the Hipparcos (van Leeuwen 2007) or *Tycho-Gaia* Astrometric Solution (*Gaia* Collaboration et al. 2016) data sets. Spectral types and luminosity classes (LCs) given in SIMBAD were also compiled, along with various ancillary notes about each star, such as whether it is a member of a double system or a spectroscopic binary, and whether it is a known variable. A number of the stars in the PM11 sample are long period variables (LPVs).

In regard to photometry the *B*–*V* colours given by PM11 were adopted here, while *V* magnitudes were acquired from the General Catalogue of Photometric Data (Mermilliod, Mermilliod, & Hauck 1997; GCPD). One photometric system that provides useful data on the evolutionary state of a red giant is the David Dunlap Observatory (DDO) system (McClure & van den Bergh 1968). Such photometry is available for a large fraction of the stars in the PM11 sample. Values of the two main colours within this system, *C*(45–48) and *C*(42–45), were obtained from McClure & Forrester (1981) where available, and in other instances were gleaned from the GCPD.

Apparent FUV magnitudes $m_{\rm FUV}$ for PM11 giants were found by searching the *GALEX* GR6/7 Data Release[a]. This was done

Author for correspondence: Graeme H. Smith, Email: graeme@ucolick.org
Cite this article: Smith GH. (2018) A correlation between *GALEX* FUV magnitude and chromospheric activity among red giant stars. *Publications of the Astronomical Society of Australia* **35**, e037, 1–13. https://doi.org/10.1017/pasa.2018.45

[a]http://galex.stsci.edu/GR6.

using the *GALEX* Catalog Search tool[b] for a search radius of 0.2 arcmin around the sky position of each star. There are 26 stars for which two values of $m_{\rm FUV}$ were returned by the position search, and for these stars the average range between the two values was 0.17 mag, with a standard deviation in the range of 0.27 mag. Seven of these 26 stars (27%) are spectroscopic binaries, although six of them do not show unduly large ranges in $m_{\rm FUV}$. One of the seven SBs with two measurements showed a difference of more than 1 mag in $m_{\rm FUV}$, a range that might be related to binary-induced variability. Omitting this star from a consideration of error estimates, the average range in $m_{\rm FUV}$ decreased from 0.17 to 0.13, with a standard deviation in the range of 0.13. Thus a typical 1σ observational error in $m_{\rm FUV}$ for the PM11 sample would seem to be ∼0.11–0.15 mag, although errors as great as ∼ 0.4 mag may be encountered. By comparison, the photometric repeatability in $m_{\rm FUV}$ is quoted by Morrissey et al. (2007) as 0.05 mag. The *GALEX* apparent FUV magnitude was used to form a colour ($m_{\rm FUV}$–B), following the approach of Smith & Redenbaugh (2010) for dwarf stars.

The basic data compiled for this paper are listed in Table 1, wherein is given the HD number of each red giant, the absolute magnitude M_V, (B–V) and ($m_{\rm FUV}$–B) colours, effective temperature and Mg II h and k flux from PM11, and a $v \sin i$ projected rotation velocity obtained as described in Section 5. In summary, the sample of red giants compiled in Table 1 comprises 177 stars, of which 38 are of an LC brighter than III. There are 42 spectroscopic binaries and 19 LPVs in the sample, identified by footnote marks in Table 1.

3. Properties of red giants in the PM11 sample

The Mg II flux parameters $\log F_{\rm mgii}$ and $\log (F_{\rm mgii}/F_{\rm bol})$ are shown versus B–V in Figures 1 and 2, respectively. Both exhibit a trend towards decreasing flux levels along the red giant sequence towards redder B–V, although the trend is stronger in the unscaled surface flux $F_{\rm mgii}$. Eye-estimates of baselines to the Mg II flux relationships with respect to B–V are shown as solid lines in Figures 1 and 2, and have the equations

$$\log (F_{\rm mgii})_b = 6.30 - 1.125(B-V) \quad (2)$$

and

$$\log (F_{\rm mgii}/F_{\rm bol})_b = -7.8 - 0.5(B-V). \quad (3)$$

One of the main objectives of Pérez Martínez et al. (2011) was to more precisely define the behaviour of this base flux level as a function of effective temperature among evolved stars (see also Judge & Stencel 1991). Spectroscopic binaries are shown as crosses in Figures 1 and 2, while LPVs are plotted as open circles. There is typically a range of ∼1 dex (or more) in $\log F_{\rm mgii}$ throughout the colour range $0.8 \leq (B-V) < 1.6$ (Figure 1). Some of the highest Mg II surface fluxes at a given B–V are found among spectroscopic binaries. The LPVs have B–$V > 1.4$ and among these there is again a range of ∼1 dex in Mg II surface flux. The behaviour of $\log (F_{\rm mgii}/F_{\rm bol})$ is rather similar, although the baseline variation with B–V is less steep.

Both $\log F_{\rm mgii}$ and $\log (F_{\rm mgii}/F_{\rm bol})$ could be used as a measure of the level of chromospheric activity at the surface of a red giant. In fact, the work of Pérez Martínez et al. (2011) just reported the unscaled flux $\log F_{\rm mgii}$. Figure 3 shows that the two parameters correlate well among the sample of PM11 giants.

Two versions of the colour–magnitude diagram (CMD) of the PM11 sample are shown in Figure 4. In the top panel the points are encoded according to the LC given in SIMBAD for each star. Filled circles correspond to stars listed as having an LC of III or III–IV, whereas open circles correspond to LC III–II, II, or I. In the bottom panel the symbols are used to highlight stars that are LPVs or members of spectroscopic binary systems. As would be expected, most of the LC III giants have absolute magnitudes of $M_V > -2.0$. However, there are perhaps five stars in Figure 4 for which SIMBAD gives an LC of III but for which the absolute magnitude is more consistent with a bright giant of class II. Model evolutionary tracks for stars in the first-ascent red giant branch (RGB) phase from the Dartmouth Stellar Evolution Programme (Dotter et al. 2008) are shown in the top panel of Figure 4 for solar metallicity stars of 1 $M_\odot$ (solid line), 2 $M_\odot$ (dotted line), and 3 $M_\odot$ (dashed line). The tracks encompass many of the PM11 stars of LC III, indicating that a significant fraction of these stars are in the hydrogen-shell-burning RGB phase of evolution. There is also a sequence of helium-core-burning stars discernible in the region of the CMD corresponding to $0.4 \leq M_V \leq 1.1$ and $0.85 \leq (B-V) \leq 1.20$. Spectroscopic binaries are spread throughout the entire distribution of points in Figure 4. Long-period variables in the PM11 sample typically have B–$V \geq 1.45$, and most are spread in absolute magnitude throughout the range $-4.5 \leq M_V \leq -0.5$.

The DDO photometry collected here is used to plot the C(45–48) versus C(42–45) two-colour diagram in Figure 5. As with the upper panel of Figure 4 the symbols denote the LC as given by the SIMBAD database. It has been well documented that the C(42–45) colour is sensitive to effective temperature, whereas the C(45–48) colour is influenced by surface gravity (McClure 1971, 1976, 1979; Tripicco & Bell 1991). For example, Janes (1975) and McClure & Forrester (1981) have shown that LC III, II, and Ib stars follow off-set sequences in Figure 5, and the PM11 sample clearly shows the brighter LC (III–II, II, and I) stars falling at higher values of C(45–48) than their LC III counterparts. As such, the two-colour diagram in Figure 5 can serve as a proxy for a Hertzsprung–Russell diagram or CMD, and can be compared with the upper panel of Figure 4. As with the previous figure, there appear to be five giants in the PM11 sample for which the DDO photometry is suggestive of a brighter LC than the III quoted in SIMBAD.[c] In both Figures 5 and the upper panel of Figure 4 there is one PM11 star that is depicted with a cross; SIMBAD did not quote an LC for this star (HD 210745), while both the DDO colours and position in the CMD are consistent with a giant that is brighter than LC III.

In summary, Figures 4 and 5 reveal that the PM11 sample consists of giants that are in a variety of evolutionary stages, with LCs of III and II being well represented, and a few giants attaining to class I. Many of the LC III stars are likely to be hydrogen-shell-burning first-ascent RGB stars with masses between 1 and 3 $M_\odot$. Stars in a more evolved core-helium-burning phase with mass less than 2.5 $M_\odot$ also seem to be present among the LC III sample. Figure 4 indicates that the LC II and I stars in the PM11 sample with absolute M_V magnitudes between −2 and −6 will have masses greater than 3 $M_\odot$. Long-period variables are candidates to be in an asymptotic giant branch phase of evolution.

4. The correlation between Mg II emission and FUV brightness

A plot of ($m_{\rm FUV}$–B) versus (B–V) for the PM11 stars is given in Figure 6. There is a considerable range in the FUV-to-B colour for giants of all spectral types and photospheric temperatures

[b] http://galex.stsci.edu/gr6/?page=mastform.

[c] These five stars are HD 352 (an eclipsing binary of the β Lyr type), HD 3712 (a double star), HD 20644, HD 57669, and HD 150798 (a double star).

https://doi.org/10.1017/pasa.2018.45 Published online by Cambridge University Press

Table 1. Red giant Mg II h and k fluxes and photometric data

HD	M_V (mag)	B–V (mag)	m_{FUV}–B (mag)	log T_{eff} (K)	log F_{mgii} (mW m^{-2})	$v \sin i$ (km s^{-1})
28[a]	1.62[c]	1.02	13.90	3.669	5.31	3.2
352[a]	–2.01	1.27	...	3.633	6.10	22.3
496	0.79	1.00	13.92	3.688	5.32	2.1
1 522	–0.68	1.19	13.64	3.660	5.18	2.5
2 261[a]	0.32[c]	1.08	13.88	3.666	5.38	1.6
3 627[a]	0.65	1.26	13.96	3.642	5.04	4.3
3 712	–2.00[c]	1.15	...	3.662	5.18	7.5
4 128	–0.32[c]	1.01	...	3.683	5.76	4.9
4 174[a]	–1.94	1.40	4.04	3.602	5.62	...
4 502[a]	0.35	1.08	10.08	3.668	6.40	38.2
6 805	0.70	1.15	...	3.661	5.12	3.7
6 860	–1.86[c]	1.56	12.41	3.589	4.90	7.2
8 512	0.89	1.05	14.10	3.679	5.23	2.7
9 053[a]	–0.78	1.52	11.26	3.593	5.15	...
9 746[a]	–0.07	1.20	...	3.635	6.64	8.2
9 927	–0.01	1.26	...	3.638	4.95	5.9
10 380	–0.70	1.31	13.55	3.630	5.12	...
12 929	0.48[c]	1.14	...	3.651	5.20	2.2
13 480[a]	0.20[c]	0.74	...	3.714	6.45	36.0
17 506	–3.11	1.56	...	3.602	4.94	6.0
18 322	0.89	1.07	14.06	3.673	5.34	2.3
18 884[b]	–1.89[c]	1.61	...	3.575	4.68	6.9
19 476	1.16	0.97	...	3.676	5.32	2.0
20 644	–1.86	1.49	...	3.604	4.62	1.4
20 720[b]	–1.43	1.59	11.69	3.572	4.85	...
23 817[a]	1.36	1.12	14.02	3.662	5.18	...
24 512	–0.67	1.57	12.38	3.582	4.88	...
25 025[b]	–0.66	1.57	12.43	3.588	4.78	...
26 967	1.08	1.07	14.16	3.664	5.18	...
27 371	0.42	0.97	...	3.697	6.48	2.9
27 697[a]	0.16	0.97	...	3.697	5.54	3.4
28 305	0.07	1.00	...	3.696	5.41	3.4
28 307[a]	0.49	0.94	...	3.696	5.80	2.8
29 139[b]	–0.68[c]	1.53	...	3.590	4.78	3.5
31 398	–3.61	1.44	12.81	3.612	4.97	3.5
31 767	–2.96	1.27	...	3.641	4.94	1.1
32 068[a]	–2.63	1.08	...	3.648	5.92	6.8
32 887	–0.79	1.44	13.20	3.611	4.91	3.0
32 918	1.32	0.98	8.93	3.675	6.76	47.1
37 160	1.40	0.94	...	3.691	5.61	0.8
39 364	1.16	0.97	13.83	3.684	5.56	1.5
39 425	0.90	1.14	...	3.667	5.26	...
39 801[b]	–5.44[c]	1.46	12.83	3.589	4.76	...
40 239[b]	–2.59	1.62	...	3.566	4.69	...
40 409	2.48	1.01	14.03	3.681	5.28	...
42 995[a]	–2.08[c]	1.57	...	3.572	4.89	...

https://doi.org/10.1017/pasa.2018.45 Published online by Cambridge University Press

Table 1. (Continued)

HD	M_V (mag)	$B–V$ (mag)	$m_{FUV}–B$ (mag)	log T_{eff} (K)	log F_{mgii} (mW m^{-2})	$v \sin i$ (km s^{-1})
43 039	0.89	1.00	...	3.671	5.37	2.5
44 478[b]	–1.38[c]	1.60	...	3.571	4.60	8.4
46 697[a]	1.86	1.09	...	3.665	6.24	16.0
47 205	2.46	1.03	...	3.676	5.44	1.6
50 310[a]	–0.73	1.19	...	3.656	5.12	2.0
50 877[b]	–4.14	1.54	...	3.609	4.84	...
52 877[b]	–5.09	1.61	...	3.587	5.00	...
54 810	1.05	1.00	...	3.678	5.45	1.2
56 855[b]	–4.26[c]	1.51	...	3.604	4.97	...
57 669	–1.92	1.18	12.84	3.655	6.05	4.5
59 693	–4.53	0.87	...	3.709	6.43	...
59 717[a]	0.04	1.49	...	3.602	4.74	...
60 414[a]	–4.16	1.03	...	3.640	6.93	...
61 772	–1.76	1.48	...	3.605	4.64	...
61 935	0.76	1.01	...	3.685	5.30	1.6
62 044[a]	1.51	1.11	...	3.667	6.64	25.7
62 345	0.44	0.92	13.75	3.707	5.45	2.8
62 509	1.07[c]	0.99	...	3.696	5.47	2.2
63 032	–3.38	1.57	...	3.593	4.96	...
63 700	–4.14	1.08	...	3.695	5.78	9.1
69 267	–1.26	1.45	...	3.611	4.95	5.3
71 369	–0.54	0.84	12.80	3.718	5.48	3.9
73 974[a]	0.58	0.87	11.71	3.715	5.98	...
76 294	–0.31	0.96	14.27	3.682	5.30	2.4
77 912	–1.93	0.97	12.05	3.710	5.84	4.4
78 647[b]	–3.91[c]	1.61	...	3.583	4.99	6.5
80 493	–0.87	1.53	12.87	3.594	4.85	6.4
81 797	–1.74[c]	1.42	...	3.619	4.88	4.8
81 817[a]	–2.86	1.38	11.20	3.622	4.97	5.5
82 210[a]	2.02	0.77	11.22	3.721	6.45	5.5
82 668	–0.90	1.51	...	3.598	4.72	...
84 441	–1.78	0.78	11.31	3.746	5.99	6.8
85 503	1.31	1.21	14.05	3.657	5.24	3.3
88 284[a]	1.00	1.00	13.55	3.697	5.24	2.0
89 388[b]	–3.46	1.47	...	3.615	5.16	...
89 484	–0.95[c]	1.12	...	3.654	5.16	2.1
89 758[a]	–1.98	1.58	12.17	3.583	4.87	7.5
90 610	–0.74	1.39	...	3.618	5.01	...
93 497	–0.09[c]	0.89	...	3.708	6.07	6.3
93 813	–0.11	1.22	13.79	3.644	5.11	5.3
94 264	1.29	1.03	13.98	3.683	4.97	2.1
95 272	0.90	1.06	13.97	3.677	5.29	2.6
95 689[a]	–1.08[c]	1.05	...	3.666	5.12	2.3
96 833	–0.38	1.13	13.94	3.662	5.06	3.3
98 262	–0.75	1.36	12.61	3.627	5.14	2.7
98 430	0.07	1.09	13.62	3.660	5.28	0.9

https://doi.org/10.1017/pasa.2018.45 Published online by Cambridge University Press

Table 1. (Continued)

HD	M_V (mag)	$B-V$ (mag)	$m_{FUV}-B$ (mag)	log T_{eff} (K)	log F_{mgii} (mW m^{-2})	$v \sin i$ (km s^{-1})
102 350	−1.06	0.85	...	3.734	5.81	5.8
104 979	0.54	0.95	13.77	3.701	5.39	1.6
106 677[a]	0.39	1.10	9.07	3.663	6.51	11.7
107 328	−0.08	1.14	13.42	3.650	5.37	2.1
107 446	−0.44	1.37	....	3.620	4.97	3.1
108 903	−0.55[c]	1.59	...	3.570	4.67	...
108 907[a]	−1.52	1.56	...	3.579	4.82	...
109 379	−0.85	0.88	12.55	3.719	5.55	3.4
111 812	0.24	0.65	...	3.770	6.45	62.8
112 300	−0.89	1.55	12.13	3.578	4.78	6.0
113 226	0.25	0.92	13.50	3.697	5.49	1.3
113 996	−0.53	1.45	13.39	3.612	4.87	4.1
115 659[a]	−0.12	0.91	13.24	3.714	5.49	3.4
116 204[a]	1.82	1.12	9.06	3.651	6.56	15.1
123 139	0.78[c]	1.00	...	3.682	5.30	1.2
124 897	−0.31[c]	1.24	...	3.641	5.36	3.4
127 665	0.29	1.28	13.90	3.640	5.09	3.6
127 700	−0.81	1.40	13.32	3.614	5.00	1.9
129 078	−1.78	1.39	13.47	3.622	4.62	...
129 456	−0.01	1.34	...	3.622	4.83	3.7
131 873	−0.94[c]	1.45	13.16	3.610	4.94	1.7
133 208	−0.48	0.93	13.28	3.694	5.33	1.4
133 216[b]	−2.21	1.65	...	3.564	4.69	...
134 505	0.73	0.91	...	3.701	5.41	...
135 722	0.62	0.95	13.77	3.693	5.47	2.4
137 759	0.79	1.16	14.24	3.657	5.20	1.1
140 573	0.61	1.16	14.08	3.662	5.15	2.8
141 714[a]	1.10	0.78	11.43	3.730	6.33	6.1
146 051	−0.87[c]	1.57	12.71	3.588	4.82	7.0
146 791	0.64	0.96	9.39	3.701	5.43	3.6
147 675	0.57	0.91	12.00	3.702	5.93	3.3
148 387	0.47[c]	0.90	13.46	3.701	5.43	2.4
148 856[a]	−1.46	0.93	12.05	3.705	5.51	3.5
150 798	−3.48[c]	1.41	...	3.626	5.26	6.4
150 997	0.87	0.90	12.63	3.701	5.82	2.0
153 210[b]	1.03	1.15	14.00	3.663	5.17	4.7
153 751[a]	−0.72	0.86	...	3.718	6.22	23.0
156 283	−2.02	1.40	13.46	3.623	4.86	2.4
157 244	−5.01	1.42	...	3.622	5.36	5.4
157 999	−2.75	1.36	12.70	3.632	5.14	3.6
159 181	−2.63	0.92	10.67	3.719	6.24	9.1
161 096	0.78	1.16	14.29	3.670	5.20	3.8
161 892	−0.10	1.18	...	3.658	5.19	...
163 588	1.11	1.17	14.15	3.654	5.21	2.3
163 770	−3.94	1.28	12.40	3.647	5.37	4.5
163 993[b]	0.71	0.92	...	3.696	5.84	3.1

https://doi.org/10.1017/pasa.2018.45 Published online by Cambridge University Press

Table 1. (Continued)

HD	M_V (mag)	$B–V$ (mag)	$m_{FUV}–B$ (mag)	log T_{eff} (K)	log F_{mgii} (mW m^{-2})	$v \sin i$ (km s^{-1})
167 618[b]	–0.43	1.57	...	3.576	4.75	...
168 723	2.00	0.93	...	3.696	5.39	2.2
169 414	1.03	1.16	...	3.660	5.24	4.4
169 916	0.77	1.02	...	3.674	5.32	...
171 443	–0.11	1.30	...	3.633	4.97	4.2
174 974	–3.34	1.23	...	3.662	5.61	...
177 716[a]	0.55	1.16	...	3.648	5.20	3.0
183 492	0.69	1.02	...	3.683	5.24	2.3
186 791	–5.09	1.46	...	3.611	5.07	3.3
187 076[a]	–1.80	1.27	...	3.614	5.70	...
188 650	–2.12	0.62	...	3.819	6.24	...
188 947	0.76	1.01	...	3.674	5.26	2.0
192 876	–2.88	0.86	...	3.707	5.94	6.7
196 171	0.79	0.99	13.92	3.680	5.31	...
197 989	0.64	1.01	...	3.674	5.31	1.7
198 700	–2.31	1.19	12.39	3.666	5.55	...
200 905[a]	–3.49	1.49	...	3.605	5.11	2.5
202 109[a]	–0.25	0.98	...	3.702	5.25	3.8
203 387	0.33	0.87	...	3.712	6.10	5.7
204 075[a]	–1.92	0.96	10.11	3.704	5.96	5.5
205 435	1.05	0.87	...	3.708	6.08	2.3
205 478[a]	2.30	1.00	13.79	3.685	5.37	...
206 778[b]	–4.24[c]	1.45	11.80	3.619	5.39	6.0
206 859	–2.93	1.07	11.91	3.676	5.77	5.6
206 952	0.79	1.09	...	3.655	5.91	...
207 089	–2.80	1.27	11.32	3.652	5.84	19.5
208 816[a]	–3.95	0.72	...	3.695	6.10	...
209 750	–1.50	0.89	11.68	3.707	5.91	7.3
210 745	–2.94	1.49	...	3.622	5.32	7.9
211 388	–2.02	1.39	13.32	3.625	4.88	3.4
211 416[a]	–1.35	1.37	12.18	3.620	5.59	1.9
213 080[b]	–0.44	1.54	...	3.576	5.52	...
216 228	0.67	1.04	...	3.685	5.94	...
216 386[b]	–1.11	1.59	11.46	3.577	5.51	...
216 489[a]	0.66	1.10	9.19	3.664	7.39	27.3
217 906[b]	–1.44[c]	1.64	...	3.564	5.36	9.7
218 356[a]	–1.32	1.23	8.81	3.641	6.89	3.3
219 615	0.61	0.90	13.69	3.693	5.90	0.4
224 427	–1.70	1.54	11.32	3.579	5.51	...

[a] Spectroscopic binary.
[b] Long-period variable.
[c] Parallax from Hipparcos.

covered by Figure 6, that is much larger than the expected observational uncertainties. Synthetic spectrum calculations based on photosphere-only model atmospheres by Findeisen et al. (2011) indicate that throughout the effective temperature range covered by the giants in the PM11 sample the FUV flux should be dominated by chromospheric and transition region emission. As such, the scatter in Figure 6 at a given ($B–V$) is expected to trace the range in stellar activity levels among the PM11 red giants.

In addition to the pronounced scatter, there seems to be an upper envelope to the locations of the data points in Figure 6.

https://doi.org/10.1017/pasa.2018.45 Published online by Cambridge University Press

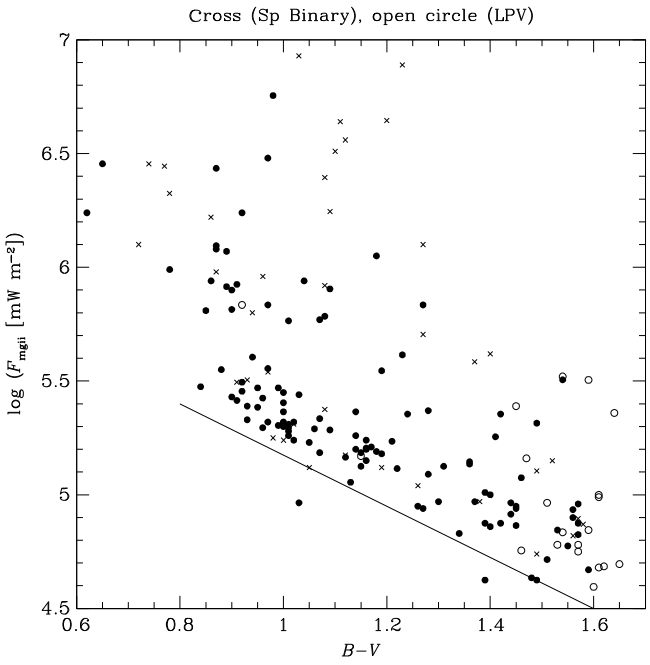

Figure 1. The surface flux of Mg II *h* and *k* emission versus *B*–*V* colour for giant stars in the PM11 sample. There is a notable decrease in the mean flux with increasing *B*–*V*, with the solid line being an eye-estimate of the lower limit to this trend. Crosses and open circles denote spectroscopic binary and LPV stars, respectively.

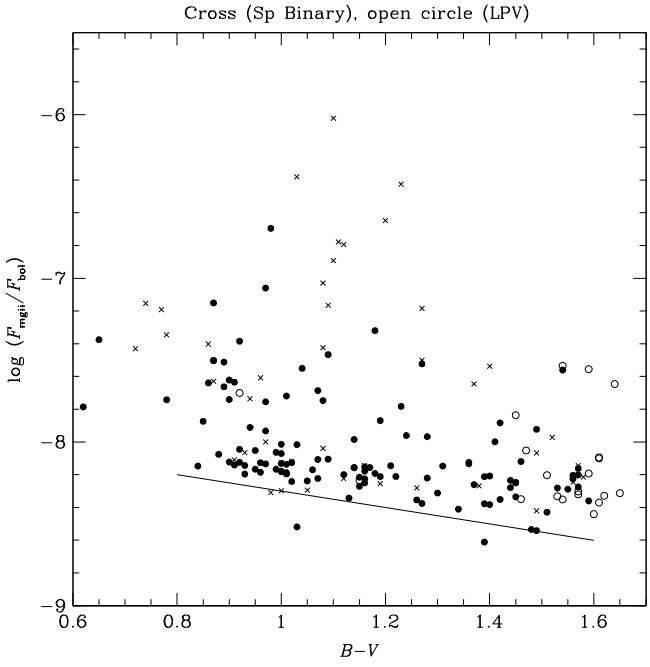

Figure 2. The normalised flux ratio log (F_{mgii}/F_{bol}) versus *B*–*V* colour for giant stars in the PM11 sample. There is a decrease in the mean flux ratio with increasing *B*–*V*, the solid line depicting an eye-estimate of the lower limit to this trend. Crosses and open circles denote spectroscopic binary and LPV stars, respectively.

Among giants at each (*B*–*V*) colour there is an empirical red limit to (m_{FUV}–*B*), the value of which varies with photospheric colour. The locus of this red envelope in Figure 6, which is denoted $(m_{FUV}–B)_e$, is defined by those giants within the PM11 sample that have the lowest FUV-to-*B* flux ratio for their spectral

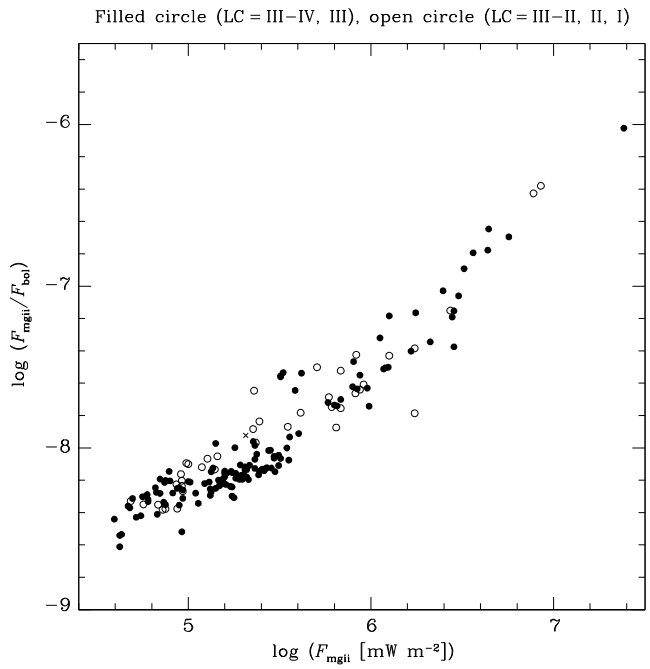

Figure 3. The normalised flux ratio log (F_{mgii}/F_{bol}) versus the surface flux of Mg II *h* and *k* emission for giant stars in the PM11 sample.

type. An eye-estimate of the upper envelope has been added to Figure 6, where it is shown by the pair of intersecting straight lines. Dwarf stars show an analogous upper-envelope phenomenon in the (m_{FUV}–*B*, *B*–*V*) diagram (Smith & Redenbaugh 2010). In reference to the red giants of the PM11 sample, the two segments of the upper-envelope locus adopted in Figure 6 correspond to

$$(m_{FUV}-B)_e = 2.25(B-V) + 11.70 \quad (4)$$

for red giants with $B-V < 1.2$, and

$$(m_{FUV}-B)_e = -4.25(B-V) + 19.5 \quad (5)$$

for the coolest PM11 giants with $(B-V) > 1.2$. By and large, it is LC III giants that define the upper envelope in Figure 6. An upper fiducial comprised of two segments seems consistent with the data, although our use of two straight lines might be a simplification of a more complicated function. The break at a colour of $(B-V) = 1.2$ ensures that all core-helium-burning stars are referenced to Equation (4), while no core-helium-burning stars should be found in the colour range covered by Equation (5).

Comparing the FUV-based colour (m_{FUV}–*B*) directly with the Mg II *h* and *k* surface flux, both in units of mW m^{-2} and scaled to the bolometric surface flux, gives the plots shown in the upper and lower panels, respectively, of Figure 7. While trends are evident in both panels there is broad scatter. One factor contributing to the scatter is the phenomenon that red giants of different (*B*–*V*) colours are associated with different upper limits to the (m_{FUV}–*B*) colour. A first-order way of taking this effect into account was experimented with by referencing the (m_{FUV}–*B*) colour of each star to the upper-envelope value $(m_{FUV}–B)_e$ given by either Equation (4) or (5) for the appropriate (*B*–*V*). The difference, denoted here as $Q(m_{FUV}–B) = (m_{FUV}–B) - (m_{FUV}–B)_e$, can serve as an FUV-excess parameter. It is defined in such a way that as the flux in the FUV band increases relative to the *B*-band flux the value of $Q(m_{FUV}–B)$ becomes more negative.

https://doi.org/10.1017/pasa.2018.45 Published online by Cambridge University Press

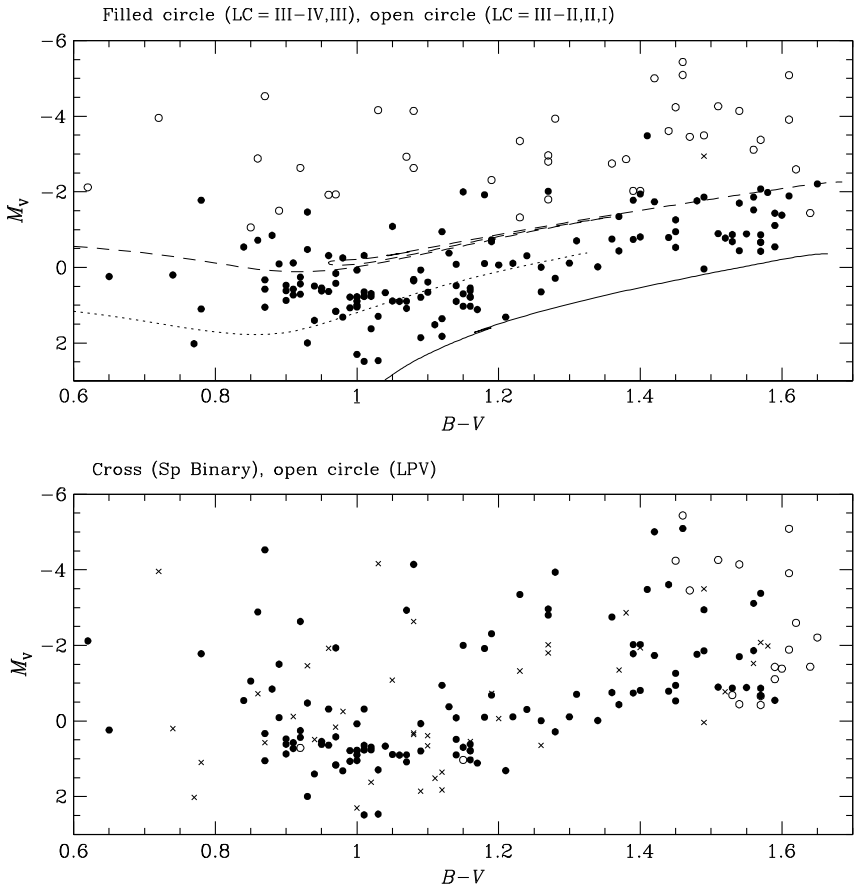

Figure 4. The CMD of giant stars in the PM11 sample. Top panel: symbols are chosen to denote LC (the one cross in this panel denotes a star for which SIMBAD did not quote an LC). A Dartmouth evolutionary track for a solar metallicity 1 $M_\odot$ model star is shown in the upper panel by a solid line. Tracks for 2 $M_\odot$ and 3 $M_\odot$ solar metallicity models are depicted with dotted and dashed lines, respectively. Bottom panel: LPVs and members of spectroscopic binary systems are represented with distinctive symbols.

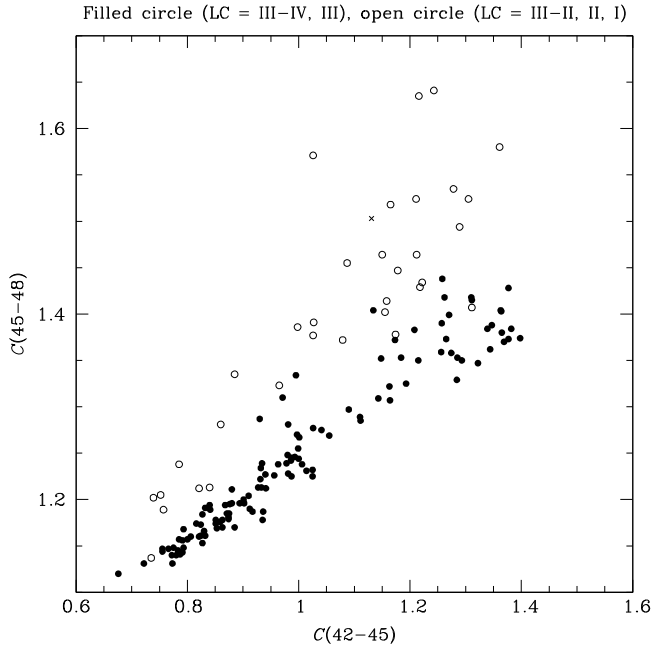

Figure 5. The DDO two-colour diagram of giant stars in the PM11 sample. Within the DDO photometric system $C(45–48)$ is sensitive to surface gravity, while $C(42–45)$ is an effective temperature indicator. Symbols are chosen to denote LC, with filled symbols corresponding to LC III giants or fainter class III–IV. The cross is a star for which SIMBAD did not specify an LC, while the position in this diagram is consistent with an LC of II or brighter.

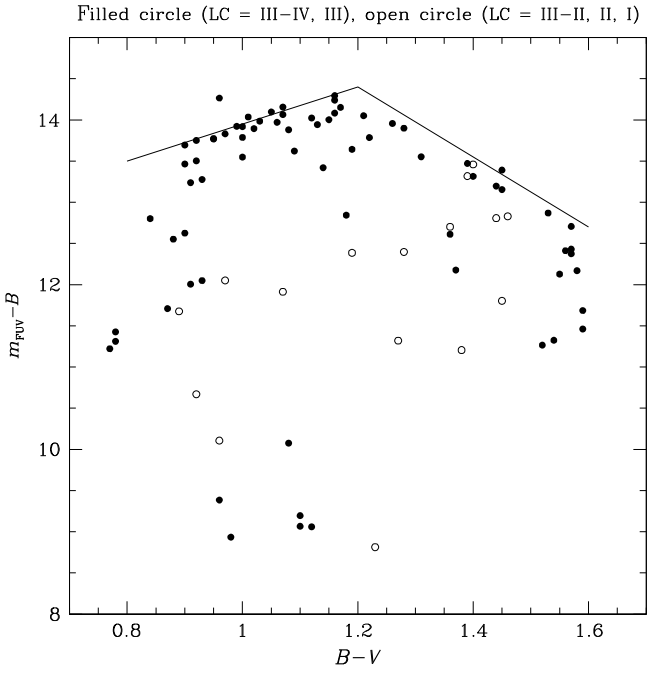

Figure 6. The FUV/blue two-colour diagram of giant stars in the PM11 sample. LC III stars (or fainter) are represented by filled circles, while giants of brighter classes are shown with open circles. The solid locus is an eye-estimate to the upper envelope of the data points and is given by Equations (4) and (5) in the text.

https://doi.org/10.1017/pasa.2018.45 Published online by Cambridge University Press

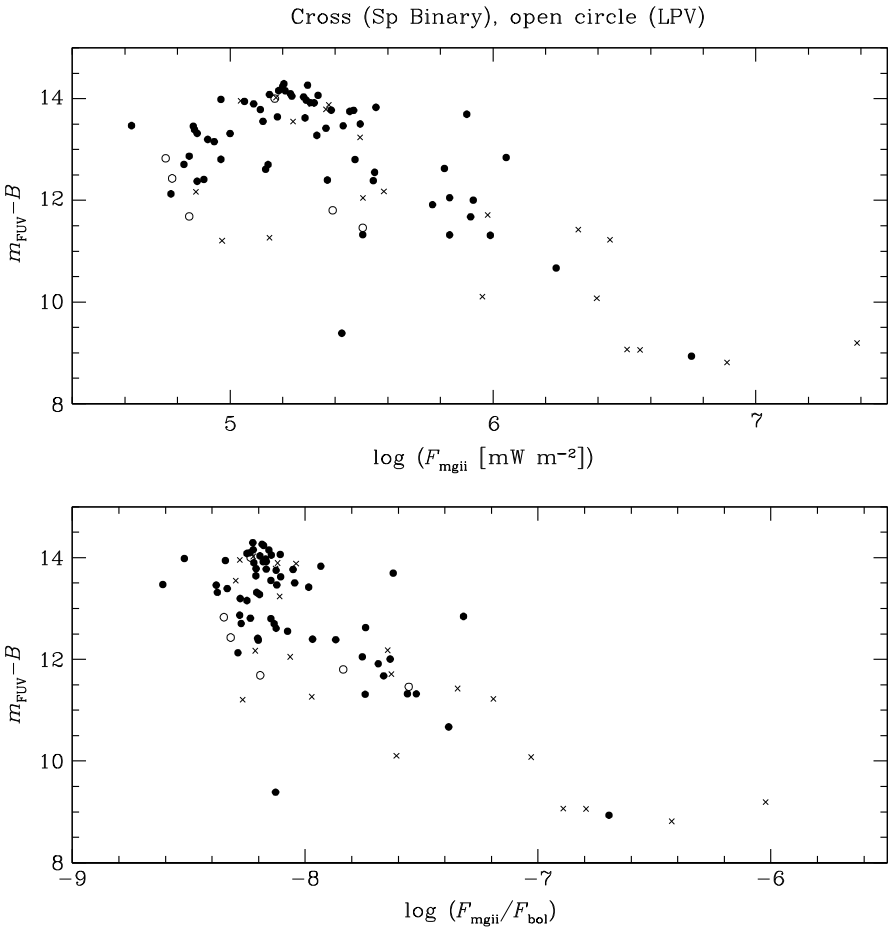

Figure 7. The (m_{FUV}–B) colour of giant stars in the PM11 sample versus two measures of the surface flux of the Mg II $h+k$ emission lines. In the top panel the surface flux in units of mW m^{-2} from the PM11 survey is plotted, whereas in the bottom panel the emission line flux has been scaled to the bolometric surface flux. Spectroscopic binaries and LPVs are depicted with crosses and open circles, respectively; all other stars are shown as filled circles.

In Figure 8 the FUV-excess $Q(m_{FUV}-B)$ is plotted versus the Mg II flux parameter log (F_{mgii}/F_{bol}) for PM11 giants in the colour range $0.70 < (B–V) < 1.20$. The crosses and open circles in this figure denote spectroscopic binary and LPV stars, respectively. Although some of the giants with the greatest FUV excess and strongest Mg II $h+k$ emission are in spectroscopic binary systems, such binaries nonetheless fall close to the sequence defined by the other stars. A correlation is evident for which the value of the Spearman rank correlation coefficient is −0.71. However, even without the envelope correction incorporated into the Q-parameter, with just a ($B–V$) colour restriction to the 0.7–1.20 range alone, ($m_{FUV}-B$) evinces a well-defined correlation against log (F_{mgii}/F_{bol}). In fact the Spearman rank correlation coefficient for this case is −0.81, higher than for the $Q(m_{FUV}-B)$ parameter. This would seem to confirm that the FUV flux of these giant stars is indeed dominated by emission originating from the chromosphere and transition region.

Correlations were also sought between FUV-excess and the surface flux log F_{mgii} within the colour range $0.70 < (B–V) < 1.20$. Once again the correlation with ($m_{FUV}-B$) was slightly tighter (Spearman rank correlation coefficient of −0.87) than with $Q(m_{FUV}-B)$ (Spearman coefficient of −0.72). In the former case a linear least-squares fit is given by the equation

$$(m_{FUV}-B) = 28.31(\pm 1.29) - 2.77(\pm 0.23) \log F_{mgii}. \quad (6)$$

This has the highest correlation coefficient of any of the four fits experimented with for PM11 stars in the colour range $0.70 < (B–V) < 1.20$. The corresponding data and the least-squares fit are shown in Figure 9.

Within the colour range $1.25 < (B–V) \leq 1.65$ the situation is slightly different. In this case correlations between Mg II flux (both surface and normalised flux) and $Q(m_{FUV}-B)$ are tighter than obtained when using ($m_{FUV}-B$) directly. The strongest correlation has a Spearman coefficient of −0.74 and corresponds to the linear fit

$$Q(m_{FUV}-B) = -17.21(\pm 2.94) - 2.02(\pm 0.36) \log (F_{mgii}/F_{bol}). \quad (7)$$

Both the data points and the fit given by Equation (7) are shown in Figure 10.

Differences in interstellar reddening could contribute to scatter in Figures 8–10. In addition, there is the possibility that chromospheric activity among red giants is intrinsically variable, either due to rotation or pulsation (e.g., Choi et al. 1995; Henry et al. 2000; Brown, Gray, & Baliunas 2008).

In order to investigate whether there might be a systematic difference in FUV-excess among stars of different LCs, Figure 11 shows a plot of absolute magnitude M_V versus the parameter

https://doi.org/10.1017/pasa.2018.45 Published online by Cambridge University Press

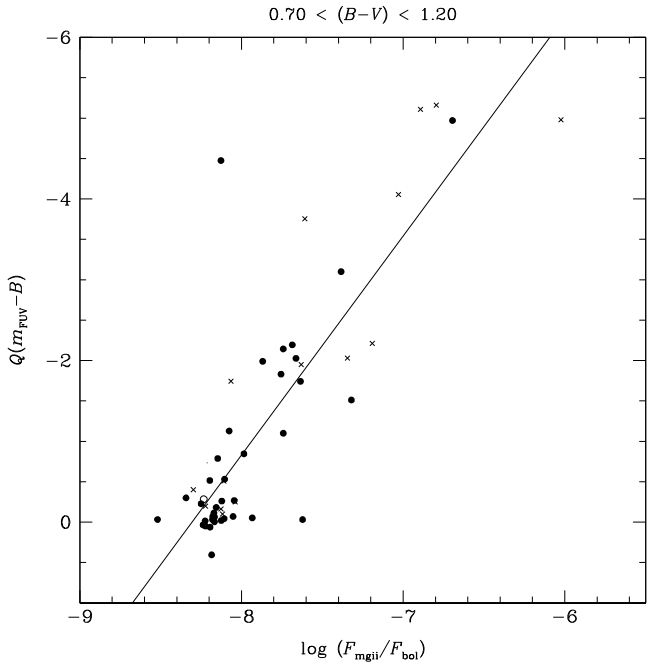

Figure 8. The FUV-excess parameter $Q(m_{\rm FUV}–B)$ versus the normalised Mg II $h+k$ flux, that is, log ($F_{\rm mgii}/F_{\rm bol}$), for giant stars in PM11 with colour in the range $0.70 < (B–V) < 1.20$. Crosses and open circles denote spectroscopic binary and LPV stars, respectively. The solid line is a linear least-squares fit.

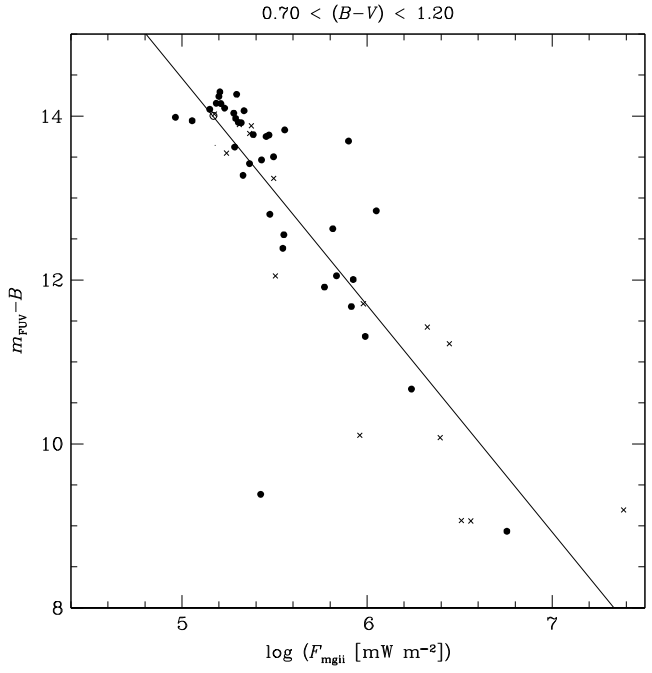

Figure 9. The FUV/blue colour ($m_{\rm FUV}–B$) versus Mg II $h+k$ surface flux log $F_{\rm mgii}$ for giant stars from PM11 with a colour of $0.70 < (B–V) < 1.20$. Crosses and open circles denote spectroscopic binary and LPV stars, respectively. The linear least-squares fit corresponding to Equation (6) from the text is shown as a solid line.

$Q(m_{\rm FUV}–B)$. Since this parameter was chosen to have two different upper-envelope fiducials according to the $B–V$ colour, Figure 11 is divided into two panels based on whether the upper envelope is given by Equation (4) or (5). Among the coolest giants

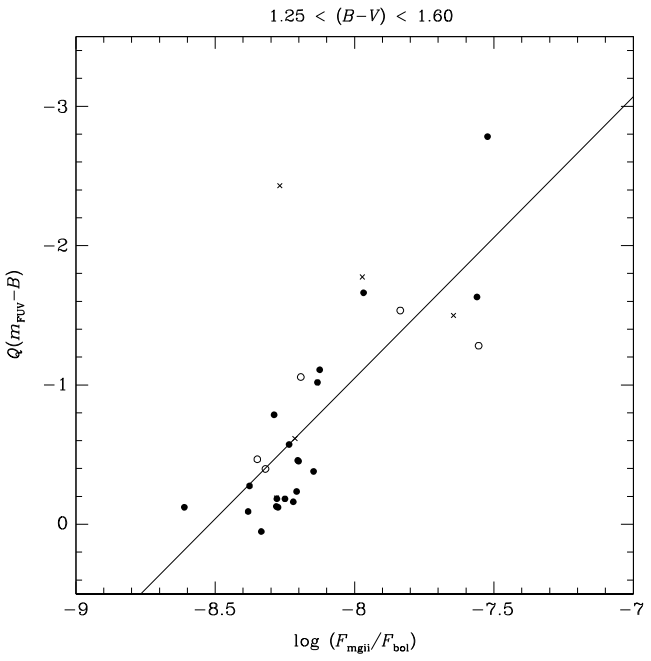

Figure 10. The FUV-excess parameter $Q(m_{\rm FUV}–B)$ versus normalised Mg II $h+k$ flux, that is, log ($F_{\rm mgii}/F_{\rm bol}$), for PM11 giants with colour in the range $1.25 < (B–V) < 1.60$. Crosses and open circles denote spectroscopic binary and LPV stars, respectively. The linear least-squares fit corresponding to Equation (7) from the text is shown as a solid line.

with $(B–V) > 1.20$ there is no systematic difference in FUV-excess exhibited by stars of LC III and those of brighter luminosities. Among the warmer giants with $(B–V) < 1.2$ those of LCs II–III or brighter have $Q(m_{\rm FUV}–B) < –1.5$, and as such exhibit greater FUV-excesses than many of the LC III stars. This can also be seen in Figure 6, although it is a result that is based on a small number of the highest-luminosity stars, and as such should be considered a tentative distinction.

5. Stellar rotation velocity and the Mg II emission

Rotation–activity relations for giant stars have been presented in the literature by a number of authors. For example, Gondoin (2005, 2007, 2014) and de Medeiros & Mayor (1995) documented correlations between X-ray surface flux and either rotation period or projected rotation speed for G and K giants. Studies of the relationships between Ca II H and K emission and rotation period or projected rotation speed among evolved stars have been carried out by Middelkoop (1982), Rutten (1987), Young, Ajir, & Thurman (1989), Strassmeier et al. (1994), and do Nascimento et al. (2003). Strassmeier et al. (2012) found a correlation between Hα-core flux and rotation period for rapidly rotating active giants in binary systems. Projected rotational velocities $v \sin i$ have been measured for many of the giants in the PM11 compendium, allowing addition of the PM11 sample to these preceding studies.

Attention to the source material for $v \sin i$ rotational speeds is restricted herein to a small number of relatively extensive catalogues or observational programmes that have appeared since 2004. Glebocki & Gnacinski (2005) compiled an extensive compendium of stellar rotation velocities, and values for many of the red giants in PM11 were gleaned from this source via the VizieR Information System (Ochsenbein, Bauer, & Marcout 2000), made available online by the CDS (Centre de Données Astronomiques

https://doi.org/10.1017/pasa.2018.45 Published online by Cambridge University Press

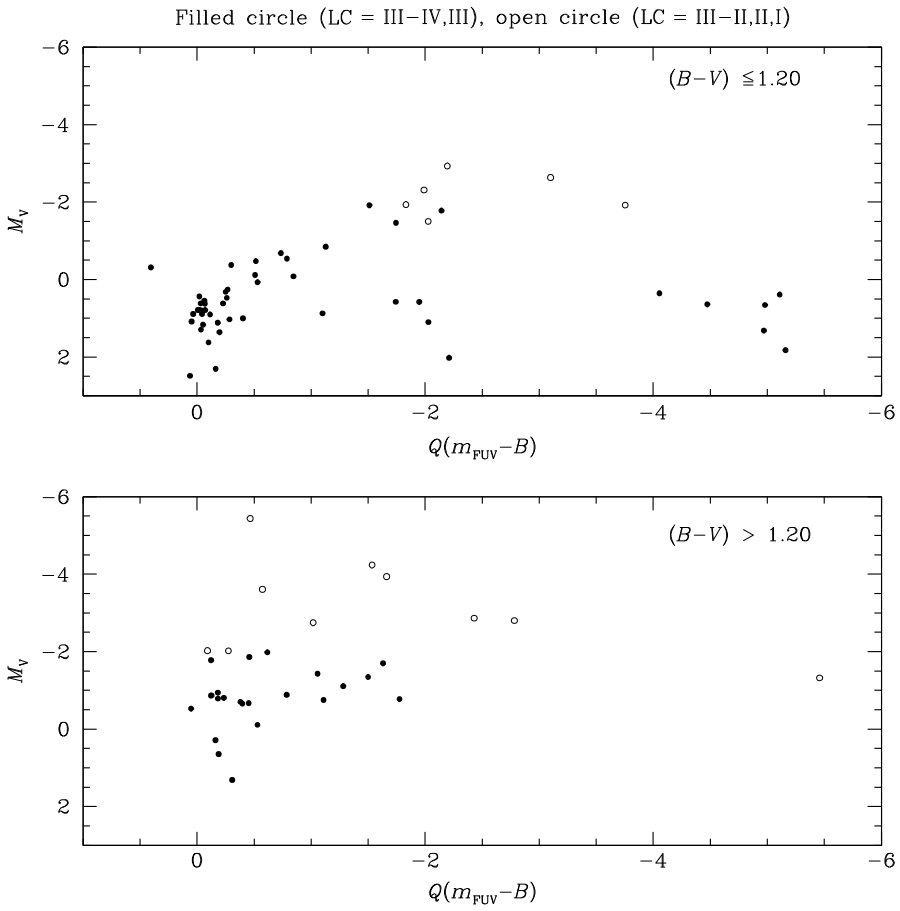

Figure 11. Absolute magnitude versus the FUV-excess parameter $Q(m_{FUV}–B)$ for the PM11 giant stars. The upper and lower panels correspond to the $B–V$ colour ranges for which the upper reference envelope used in the $Q(m_{FUV}–B)$ parameter is given by Equations (4) and (5), respectively. LC III stars (or fainter) are shown as filled circles, while open circles depict brighter LCs (as given in the SIMBAD database).

de Strasbourg). Data from this source were supplemented with more recent results from the observational programmes of Torres et al. (2006), Schroeder, Reiners, & Schmitt (2009), Jones et al. (2011), and particularly Massarotti et al. (2008) and Jofré et al. (2015). Where values of $v \sin i$ were available from one or more of these programmes plus the Catalogue of Glebocki & Gnacinski (2005) a straight unweighted average has been adopted. All $v \sin i$ values used were based on measured detections and not upper limits. Of the giants in Table 1 for which values of $v \sin i$ are listed there are 45 stars for which these values are based on measurements from two sources. The average range between the $v \sin i$ measurements in these cases is 1.9 km s^{-1}. Furthermore, there are 16 stars for which the tabulated values of $v \sin i$ are based on three measurements from the literature. In these cases, the average range in measured velocities is 2.3 km s^{-1}. Taken together, a standard deviation of 1.3–1.7 km s^{-1} seems indicated for the uncertainty in the rotation velocity measurements from the adopted literature sources.

Projected rotational speeds for the PM11 giants are shown in Figures 12 and 13 in which the surface flux $\log F_{mgii}$ (mW m^{-2}) and the normalised flux $\log (F_{mgii}/F_{bol})$ are plotted, respectively, against $v \sin i$ (in units of km s^{-1}). Symbols are used to distinguish between giants of different colours, such that open circles denote $0.80 \leq (B–V) \leq 0.99$, filled circles $1.00 \leq (B–V) \leq 1.19$, and open triangles $1.20 \leq (B–V) \leq 1.39$. There is a broad tendency for the highest Mg II fluxes to be associated with giants having $\log (v \sin i) > 0.8$, but for any value of projected speed less than this a substantial range in Mg II flux is observed. Perhaps part of this scatter might be attributable to differences in the inclination angle i among the PM11 giants, and some to observational uncertainties in the $v \sin i$ measurements. Intrinsic variability in chromospheric activity may also contribute. Another factor is that for the most slowly rotating giants of largest radii a substantial difference in rotation period (and hence any rotation-induced component of chromospheric activity) may translate to only a small, and difficult to detect, difference in $v \sin i$.

At the lowest Mg II fluxes where $\log F_{mgii}$ (mW m^{-2}) < 5.6 some separation of giants according to $(B–V)$ colour is apparent in Figure 12, such that as $(B–V)$ becomes redder the lowest surface flux attained by giant stars decreases. This trend is in accord with the baseline indicated in the corresponding plot of surface Mg II flux versus $(B–V)$ in Figure 1. Within Figure 12 the reddest giants with $(B–V) = 1.2$–1.4 appear to follow a sequence that is offset from the warmest giants with $(B–V) = 0.8$–1.0. The correlation between $\log F_{mgii}$ and rotation speed appears to vary with the effective temperature of evolved giants. This is consistent with previous findings by Rutten (1987) and Strassmeier et al. (1994), who found

https://doi.org/10.1017/pasa.2018.45 Published online by Cambridge University Press

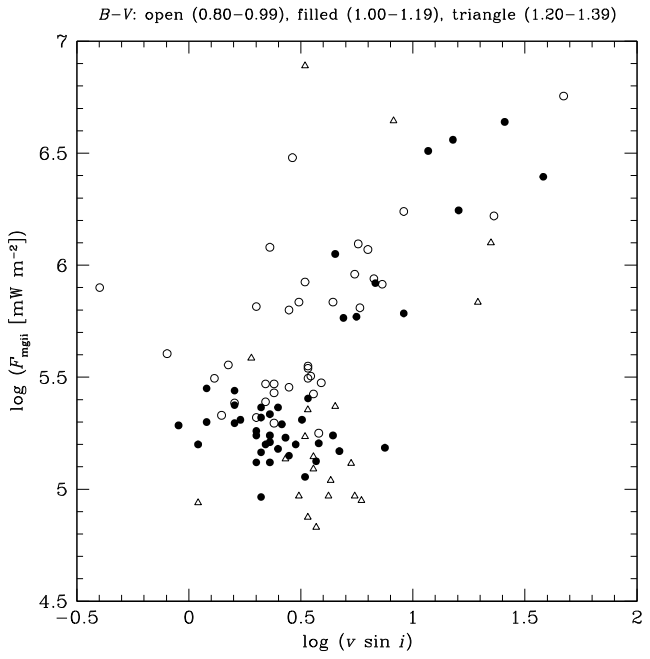

Figure 12. Surface Mg II $h+k$ flux log $F_{\rm mgii}$ (mW m^{-2}) versus projected rotation speed (km s^{-1}) for giant stars from PM11 with colour in the range $0.80 \leq (B–V) \leq 1.39$. Different symbols are used to denote different subintervals within this broader colour range: (open circles) $0.80 \leq (B–V) \leq 0.99$; (filled circles) $1.00 \leq (B–V) \leq 1.19$; (open triangles) $1.20 \leq (B–V) \leq 1.39$.

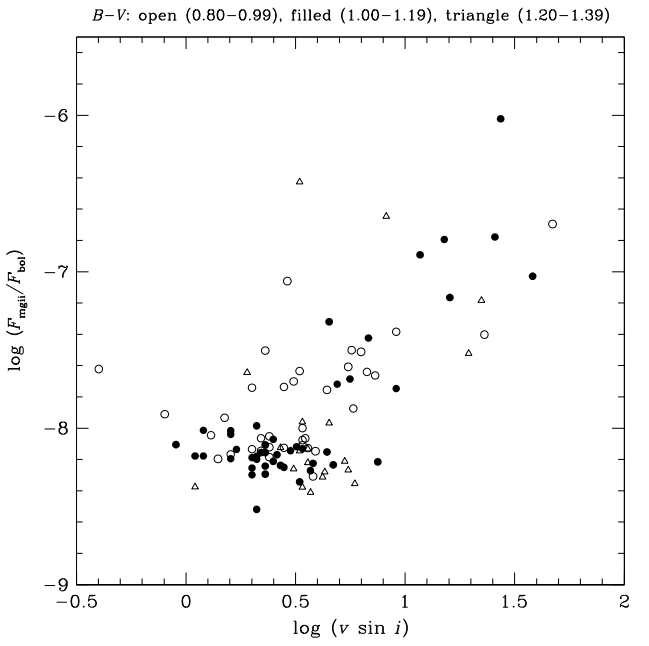

Figure 13. Normalised Mg II $h+k$ flux, that is, log ($F_{\rm mgii}/F_{\rm bol}$), versus projected rotation speed (km s^{-1}) for giant stars from PM11 with $0.80 \leq (B–V) \leq 1.39$. Symbols denote different colour subranges: (open circles) $0.80 \leq (B–V) \leq 0.99$; (filled circles) $1.00 \leq (B–V) \leq 1.19$; (open triangles) $1.20 \leq (B–V) \leq 1.39$.

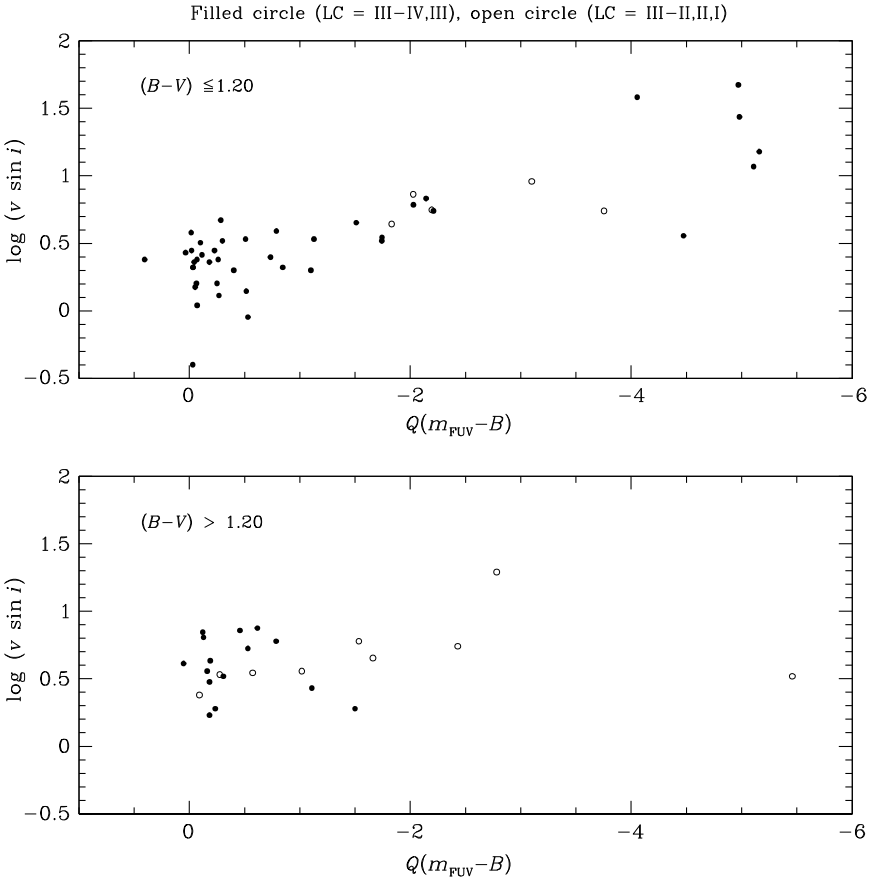

Figure 14. Projected rotation speed (km s^{-1}) versus the FUV-excess parameter $Q(m_{\rm FUV}–B)$ for the PM11 giant stars. Upper and lower panels correspond to the range in $B–V$ for which the upper fiducial used in the $Q(m_{\rm FUV}–B)$ parameter is given by Equations (4) and (5), respectively. LC III stars (or fainter) are shown as filled circles, while open circles depict brighter LCs (as given in the SIMBAD database).

https://doi.org/10.1017/pasa.2018.45 Published online by Cambridge University Press

a colour dependence in the relation between Ca II H and K emission and both the rotation period and the projected rotation speed.

When the normalised flux ratio is considered in Figure 13, giants of different colours intermingle more than in Figure 12. In particular, the minimum flux ratio of $\log(F_{\rm mgii}/F_{\rm bol}) \approx -8.2 \pm 0.1$ shows little variation with $(B–V)$ colour. Nonetheless, there is still some offset between the average positions of the warmest and coolest giants at the lowest Mg II flux levels.

A correlation is found between the projected rotation speed and FUV-excess for red giants with $(B–V) < 1.20$, as shown in the upper panel of Figure 14. There is scatter nonetheless, and the correlation is largely driven by those giants with an FUV-excess of more than 0.5 magnitudes. Among the coolest giants in the PM11 sample, as shown in the lower panel of Figure 14, there is little evidence of a rotation versus FUV-excess correlation, although the number of stars in the lower panel of Figure 14 with a Q-excess greater than 0.5 mag is relatively small.

6. Summary

As is the case with dwarf stars, $(m_{\rm FUV}–B)$ is shown to correlate with the degree of chromospheric activity among late-type evolved stars having $B–V$ colour within the range $0.8 \leq (B–V) \leq 1.2$, and even among cooler giants. In the present paper the FUV-excess has been correlated against flux in the λ2800 Mg II $h + k$ emission lines for evolved stars with LCs typically ranging from III to II. By comparison, in the work of Smith & Redenbaugh (2010) and Findeisen et al. (2011) on dwarf stars, the FUV-excess was shown to correlate with flux in the Ca II H and K emission lines. Among giants of a comparable $B–V$ a spread of up to ∼5 mag has been found in $(m_{\rm FUV}–B)$, although the majority of giants in the PM11 sample fall within a range of 3 mag in the FUV-excess parameter $Q(m_{\rm FUV}–B)$. This is comparable to the range seen among dwarfs within the colour interval $0.8 \leq (B–V) \leq 1.0$ by Smith & Redenbaugh (2010).

Within the literature homogeneous measurements of chromospheric emission line strengths tend to be more numerous for dwarf stars than giants. This is particularly true of the Ca II H_2 and K_2 lines, where high-resolution spectroscopic searches for exoplanets via radial velocity techniques have greatly expanded measurements of Ca II emission among dwarf stars (e.g., da Silva et al. 2011; Butler et al. 2017). Given the correlations shown in the present paper, the possibility is suggested that *GALEX* FUV magnitudes could be applied to a systematic study of stellar activity among cool giant stars. Such a project could utilise broadband *GALEX* activity data for thousands of giants to complement spectroscopic studies of individual chromospheric lines, such as those of Simon & Drake (1989) and Pérez Martínez et al. (2011), that have comprised ∼200 or fewer giants.

Acknowledgements. The author gratefully acknowledges the support of award AST-1517791 from the National Science Foundation of the United States. This research has made use of the SIMBAD database, operated at CDS, Strasbourg, France. In addition, this research made use of the VizieR catalogue access tool, CDS, Strasbourg, France. The original description of the VizieR service was published by Ochsenbein et al. (2000). We thank the referee for a helpful report on the original version of this paper.

References

Brown, K. I. T., Gray, D. F., & Baliunas, S. L. 2008, ApJ, 679, 1531
Butler, R. P., et al. 2017, AJ, 153, 208
Choi, H.-J., Soon, W., Donahue, R. A., Baliunas, S. L., & Henry, G. W. 1995, PASP, 107, 744
da Silva, J. G., Santos, N. C., Bonfils, X., Delfosse, X., Forveille, T., & Udry, S. 2011, A&A, 534, A30
de Medeiros, J. R., & Mayor, M. 1995, A&A, 302, 745
do Nascimento, J. D. Jr., Canto Martins, B. L., Melo, C. H. F., Porto de Mello, G., & De Medeiros, J. R. 2003, A&A, 405, 723
Dotter, A., Chaboyer, B., Jevremović, D., Kostov, V., Baron, E., & Ferguson, J. W. 2008, ApJS, 178, 89
Findeisen, K., Hillenbrand, L., & Soderblom, D. 2011, AJ, 142, 23
Gaia Collaboration, et al. 2016, A&A, 595, A2
Gaia Collaboration, et al. 2018, A&A, 616, A1
Glebocki, R., & Gnacinski, P. 2005, The Catalogue of Rotational Velocities of Stars, European Space Agency, SP-560, 71
Gondoin, P. 2005, A&A, 444, 531
Gondoin, P. 2007, A&A, 464, 1101
Gondoin, P. 2014, in Magnetic Fields Throughout Stellar Evolution, Proceedings IAU Symposium No. 302, ed. P. Petit, M. Jardine, & H. Spruit (Cambridge: Cambridge University Press), p. 377
Henry, G. W., Fekel, F. C., Henry, S. M., & Hall, D. S. 2000, ApJS, 130, 201
Janes, K. A. 1975, ApJS, 29, 161
Jofré, E., Petrucci, R., Saffe, C., Saker, L., de la Villarmois, E. A., Chavero, C., Gómez, M., & Mauas, P. J. D. 2015, A&A, 574, 50
Jones, M. I., Jenkins, J. S., Rojo, P., & Melo, C. H. F. 2011, A&A, 536, 71
Judge, P. G., & Stencel, R. E. 1991, ApJ, 371, 357
Lindegren, L., et al. 2018, A&A, 616, A2
Massarotti, A., Latham, D. W., Stefanik, R. P., & Frogel, J. 2008, AJ, 135, 209
McClure, R. D. 1971, in Spectral Classification and Multicolour Photometry, IAU Symposium No. 50, ed. C. Fehrenbach, & B. E. Westerlund (Dordrecht: Reidel), p. 162
McClure, R. D. 1976, AJ, 81, 182
McClure, R. D. 1979, Dudley Observatory Report, 14, 83
McClure, R. D., & Forrester, W. T. 1981, Pub DAO, 15, 14
McClure, R. D., & van den Bergh, S. 1968, AJ, 73, 313
Mermilliod, J.-C., Mermilliod, M., & Hauck, B. 1997, A&AS, 124, 349
Middelkoop, F. 1982, A&A, 113, 1
Morrissey, P., et al. 2005, ApJ, 619, L7
Morrissey, P., et al. 2007, ApJS, 173, 682
Murgas, F., Jenkins, J. S., Rojo, P., Jones, H. R. A., & Pinfield, D. J. 2013, A&A, 552, A27
Ochsenbein, F., Bauer, P., & Marcout, J. 2000, A&AS, 143, 23
Pérez Martínez, M. I., Schröder, K.-P., & Cuntz, M. 2011, MNRAS, 414, 418
Rutten, R. G. M. 1987, A&A, 177, 131
Schroeder, C., Reiners, A., & Schmitt, J. H. M. M. 2009, A&A, 493, 1099
Shkolnik, E. L., & Barman, T. S. 2014, AJ, 148, 64
Shkolnik, E. L., Rolph, K. A., Peacock, S., & Barman, T. S. 2014, ApJ, 796, L20
Smith, G. H., Hargrave, M., & Eckholm, E. 2017, PASA, 34, 49
Smith, G. H., & Redenbaugh, A. K. 2010, PASP, 122, 1303
Simon, T., & Drake, S. A. 1989, ApJ, 346, 303
Strassmeier, K. G., Handler, G., Paunzen, E., & Rauth, M. 1994, A&A, 281, 855
Strassmeier, K. G., Weber, M., Granzer, T., & Järvinen, S. 2012, AN, 333, 663
Torres, C. A. O., Quast, G. R., da Silva, L., de La Reza, R., Melo, C. H. F., & Sterzik, M. 2006, A&A, 460, 695
Tripicco, M. J., & Bell, R. A. 1991, AJ, 102, 744
van Leeuwen, F. 2007, A&A, 474, 653
Wenger, M., et al. 2000, A&AS, 143, 9
Young, A., Ajir, F., & Thurman, G. 1989, PASP, 1017

https://doi.org/10.1017/pasa.2018.45 Published online by Cambridge University Press